The OS of GBM subgroup in arms A ($n = 40$, 28 death) and B ($n = 41$, 27 death) was 19.0 (95 % CI 15.2–33.3) and 19.5 months (95 % CI 15.8–29.2), respectively ($p = 0.90$) (Fig. 2f). The %2-year survival in arms A and B was 48 and 41 %, respectively. The OS of AA subgroup in arms A ($n = 15$, 7 death) and in arm B ($n = 15$, 8 death) was 35.4 [95 % CI 15.7–not estimated (NE)] and 27.4 months (95 % CI 17.8–NE), respectively ($p = 0.88$) (Fig. 2g). There were no differences between the arms of any subgroup.

In the subgroups defined by central pathology review, the OS of GBM in arm A ($n = 37$, 28 death) and in arm B ($n = 40$, 29 death) was 16.6 (95 % CI 13.3–29.5) and 18.7 months (95 % CI 15.4–23.4), respectively ($p = 0.92$) (Fig. 2h). The %2-year survival in arms A and B was 38 and 34 %, respectively. The OS of AA and AOA in arm A ($n = 9$, 3 death) and B ($n = 12$, 4 death) was 33.3 months (95 % CI 15.7–33.3) and NE, respectively ($p = 0.83$).

Among the 70 total deaths, 31/35 (88.6 %) patients in arm A and 32/35 (91.4 %) in arm B experienced neuronal death of an original tumor. One patient (2.9 %) in arm A and 2 (5.7 %) patients in arm B contracted treatment-related pneumonia and died from that illness. Other causes of death were pulmonary embolism (1), pneumonia (2), and unknown (1).

Toxicity

Toxicity was assessed in 110 patients receiving initial therapy and in 73 patients receiving adjuvant chemotherapy. The most frequent grade 3/4 toxicities, experienced by more than 10 % of patients, were hematologic, neurologic, gastrointestinal, and hepatic AEs (Table 4). Patients in both arms frequently experienced leukopenia and neutropenia; more than half of the patients in arm B experienced these AEs during adjuvant therapy as well as during initial therapy. More than 40 % of patients in arm A also experienced these hematologic events even during adjuvant therapy. Grade 4 neutropenia was observed in 5.6 and 39.3 % of patients in arms A and B during initial chemoradiotherapy and 11.1 and 15.6 % during adjuvant therapy. Grade 3/4 nausea and anorexia were seen in 10.7 and 16.1 % of patients in initial therapy in arm B, but were rare in the adjuvant-therapy subgroups in both arms. One patient in arm B had cerebral infarction. Extrapyramidal signs, including tremors or involuntary movements, occurred in 2 patients in each arm.

Grade 3/4 pneumonitis occurred in 1 patient in arm A and 2 in arm B during the entire treatment period. Opportunistic infections—including 2 cases of *Pneumocystis jirovecii* pneumonia (PCP), 1 case of oral candidiasis, and 2 case of herpes zoster—occurred in arm B. One patient (1.8 %) in arm A and 2 (3.6 %) patients in arm B died from treatment-related pneumonia, and 1 of these patients in arm B had PCP. One patient in arm B died from sepsis and acute respiratory distress syndrome after initial therapy. One patient in arm A died from pulmonary embolism before starting chemoradiotherapy, and 1 patient in arm A and 2 patients in arm B died from pneumonia following tumor progression.

Radiation necrosis was observed in 2 out of 54 (3.7 %) patients in arm A and 1 out of 56 (1.8 %) patients in arm B. During surgery, 1 patient in arm A was found to have radiation necrosis. Pseudo-progression within 3 months after chemoradiotherapy was not suspected in any patient.

Discussion

This study aimed to evaluate the efficacy and safety of treatment with ACNU + PCZ compared to ACNU alone as concomitant chemoradiotherapy against AA and GBM. We found no obvious differences in OS or PFS for AA and GBM between the treatment groups, but patients treated with ACNU + PCZ experienced more adverse effects than those treated with ACNU alone. TMZ is an effective regimen for malignant gliomas with less toxicity than our ACNU regimens, but it was not approved in Japan when this study began. At the end of the phase II part of this study, TMZ became available even in Japan, so this study was terminated at that point.

Methylguanine DNA methyltransferase is a major DNA repair protein and is implicated in resistance of glioma cells to alkylating agents [13]. Transcriptional silencing by MGMT promoter methylation results in inhibition of MGMT expression [14], and thus MGMT promoter methylation is strongly associated with survival in glioma patients treated with either nitrosourea or TMZ [15–17]. The status of the promoter of MGMT in primary tumors was frequently observed to change from methylated to unmethylated in recurrent tumors following ACNU or TMZ treatment [18, 19], which constitutes one of the mechanisms behind malignant gliomas' resistance to nitrosourea and TMZ. The rationale for treatment with ACNU + PCZ is that daily application of PCZ depletes MGMT activity, increasing sensitivity of AA and GBM to ACNU. Dose-dense TMZ therapy based on the theory of depletion of MGMT [20, 21], or BCNU or TMZ with direct inhibition of MGMT by O^6-benzylguanine [22, 23] has been shown in previous studies to be effective for GBMs. However, there was no difference in OS found between standard and dose-dense TMZ for newly diagnosed GBMs [20].

While we were conducting this study, the European Organization for Research and Treatment of Cancer (EORTC) Brain Tumor and Radiotherapy Groups and the

Table 4 Toxicity

Grade 3/4 adverse events	Initial therapy with RT ($n = 110$) (%)		Adjuvant therapy ($n = 73$) (%)	
	Arm A	Arm B	Arm A	Arm B
Hematologic				
Leukopenia	38.9	73.2	40.5	69.4
Neutropenia	38.9	76.8	44.4	56.3
Thrombocytopenia	5.6	50.0	40.5	50.0
Anemia	0	8.9	10.8	8.3
Neurologic				
Seizure	9.3	7.1	5.4	8.8
Speech impairment	11.1	10.7	5.4	2.9
Neuropathy-motor	11.1	12.5	0	0
Extrapyramidal sign	0	0	5.4	2.7
Pulmonary (pneumonitis)	0	3.6	2.7	0
Gastrointestinal				
Nausea	0	10.7	0	0
Anorexia	1.9	16.1	0	2.9
Hepatic				
AST	3.7	12.5	2.9	2.9
ALT	3.7	16.1	2.9	8.8
Total bilirubin	1.9	5.4	0	0
Renal (creatinine)	0	0	0	0
Metabolic				
Hyponatremia	1.9	8.9	5.9	2.9
Hypokalemia	1.9	7.1	2.9	2.9
Fever	0	3.6	0	0
Dermatologic: erythema	3.7	5.4	0	2.9

National Cancer Institute of Canada (NCIC) Clinical Trials Group (EORTC/NCIC TMZ study) reported, in 2005, that RT + TMZ significantly prolonged the survival of GBM patients compared to RT alone [24]. The median PFS, OS, and 2-year survival for RT + TMZ were 6.9, 14.6 months, and 26.5 %, respectively [24]. Although our results compared favorably with the EORTC/NCIC TMZ study, the PFS of RT + ACNU alone for GBMs in our ITT population and in GBM subgroups in central pathology review were 6.2 and 5.1 months, shorter than those from the EORTC/NCIC TMZ study. Since more than half of the patients in our study underwent TMZ treatment following disease progression, it is possible that TMZ rescued these patients with progression after ACNU regimens and prolonged the survival of these patients.

The incidence of grade 3/4 hematologic AEs—such as leukopenia, neutropenia, and thrombocytopenia—were reported to be 5, 4, and 11 %, respectively, in adjuvant TMZ therapy in the EORTC/NCIC TMZ trial [24]. Compared to TMZ, even ACNU alone caused severe hematologic AEs in 40 % of the patients in our study, and most of those patients in both arms discontinued the treatment protocol due to AEs or patient refusal related to AEs. It is noteworthy that approximately 30 % of patients in both arms failed to start adjuvant chemotherapy. The low completion rate of our protocol might explain the lack of differences in PFS and OS between the arms. After 2 patients in arm B experienced PCP, prophylactic use of cotrimoxazole (trimethoprim–sulfamethoxazole) against PCP was recommended in this study and was found to be useful.

Radiation necrosis has been reported in 2.5–21 % of patients undergoing chemoradiotherapy against malignant gliomas [25]. This complication was observed in 2.7 % of the patients in our study, but was tolerable. "Pseudo-progression" is the phenomenon of transient early disease progression after treatment with chemoradiotherapy consisting of TMZ for GBM progressive and enhancing lesions, as shown on MRI images taken immediately after treatment [25]. No patients in our study were suspected of pseudo-progression within 6 months after beginning chemoradiotherapy.

In general, the difference in histological diagnosis for local versus central pathology review is a major problem in the conduct of clinical trials on gliomas [26]. In our study, the concordance of GBM and AA between local and central diagnosis was low, but nearly identical to previous reports. In the EORTC/NCIC TMZ trial, central pathology review was performed in 85 % of cases, which confirmed the diagnosis of GBM in 93 % of the reviewed cases; 3 % had AA or AOA. In the phase III study of RT versus RT + BCNU + dibromodulcitol (EORTC 26882), of the 193 cases of AA diagnosed by the local pathologist, 176 were reviewed by the central pathologist. At review, 61 patients (35 %) were diagnosed with AA, 13 (8 %) with AOA, 4 (2 %) with AO, 44 (25 %) with GBM, 41 (23 %) with low-grade gliomas, and 13 (7 %) with another diagnosis [27].

The WHO classification system reflects the prognoses depending on grade I–IV tumors, or astrocytic or oligodendroglial tumors. However, it is based on morphological descriptions and contains subjective elements; thus, interobserver variation occurs. The boundaries between grades II, III, and IV in gliomas are unclear, and there is a trend toward a more frequent diagnosis of oligodendroglial tumors [28]. Central pathological review before inclusion of a patient into clinical study is ideal, but it is very difficult to complete for aggressive grade III/IV tumors. Even if central review before enrollment is difficult in a multi-institutional setting, it is indispensable to perform post hoc central review at least in order to appropriately interpret the results of clinical studies of gliomas. A consensus meeting might also be useful before commencing clinical studies in order to gain concordance between local and central diagnoses. More objective classification of tumors based on

genotype, such the IDH1/2 mutation or 1p/19q codeletion, should be included in at least the stratification factor and subgroup analysis.

Conclusions

No significant differences in OS or PFS were found between ACNU alone and ACNU + PCZ in either AA or GBM. We found that ACNU + PCZ treatment was more toxic in our treatment schedule. Therefore, we conclude that the addition of PCZ to ACNU was not beneficial for newly diagnosed, high-grade astrocytomas as compared to ACNU alone. Considering the greater number of AEs associated with ACNU regimens, RT + TMZ should serve as a standard therapeutic regimen in the treatment of newly diagnosed AA and GBM.

Acknowledgments We thank all the members of the JCOG Brain Tumor Study Group and the staff of the JCOG Data Center. We appreciate Dr. Nobuaki Funata and Dr. Toru Iwaki for pathological review, Dr. Satoshi Ishikura for quality assurance of radiation therapy, and Dr. Hiroshi Katayama, Dr. Kenichi Nakamura, and Mr. Hidenobu Yamada for review of the manuscript. This work was supported in part by the National Cancer Center Research and Development Fund (23A-16 and 23A-20), the Health and Labour Sciences Research Grants (H14-032, H15-025, H16-005, H17-005), and the Grant-in Aid for Cancer Research (20S-4, 20S-6) from the Ministry of Health, Labour and Welfare.

Conflict of interest The authors declare that they have no conflict of interest.

References

1. The Committee of Brain Tumor Registry of Japan (2003) Report of brain tumor registry of japan (1984–2000) 12th edition. Neurol Med Chir (Tokyo) 49(Suppl):1–101
2. Glioma Meta-analysis Trialists (GMT) Group (2002) Chemotherapy in adult high-grade glioma: a systematic review and meta-analysis of individual patient data from 12 randomised trials. Lancet 359(9311):1011–1018. doi:10.1016/S0140-6736(02)08091-1
3. Matsutani M, Nakamura O, Nakamura M, Nagashima T, Asai A, Fujimaki T, Tanaka H, Ueki K, Tanaka Y (1994) Radiation therapy combined with radiosensitizing agents for cerebral glioblastoma in adults. J Neurooncol 19(3):227–237
4. Wolff JE, Berrak S, Koontz Webb SE, Zhang M (2008) Nitrosourea efficacy in high-grade glioma: a survival gain analysis summarizing 504 cohorts with 24193 patients. J Neurooncol 88(1):57–63. doi:10.1007/s11060-008-9533-5
5. Takakura K, Abe H, Tanaka R, Kitamura K, Miwa T, Takeuchi K, Yamamoto S, Kageyama N, Handa H, Mogami H et al (1986) Effects of ACNU and radiotherapy on malignant glioma. J Neurosurg 64(1):53–57. doi:10.3171/jns.1986.64.1.0053
6. Pegg AE (1990) Mammalian O^6-alkylguanine-DNA alkyltransferase: regulation and importance in response to alkylating carcinogenic and therapeutic agents. Cancer Res 50(19):6119–6129
7. Silber JR, Bobola MS, Ghatan S, Blank A, Kolstoe DD, Berger MS (1998) O^6-methylguanine-DNA methyltransferase activity in adult gliomas: relation to patient and tumor characteristics. Cancer Res 58(5):1068–1073
8. Valavanis C, Souliotis VL, Kyrtopoulos SA (1994) Differential effects of procarbazine and methylnitrosourea on the accumulation of O^6-methylguanine and the depletion and recovery of O^6-alkylguanine-DNA alkyltransferase in rat tissues. Carcinogenesis 15(8):1681–1688
9. Souliotis VL, Kaila S, Boussiotis VA, Pangalis GA, Kyrtopoulos SA (1990) Accumulation of O^6-methylguanine in human blood leukocyte DNA during exposure to procarbazine and its relationships with dose and repair. Cancer Res 50(9):2759–2764
10. Wedge SR, Porteus JK, May BL, Newlands ES (1996) Potentiation of temozolomide and BCNU cytotoxicity by O(6)-benzylguanine: a comparative study in vitro. Br J Cancer 73(4):482–490
11. Therasse P, Arbuck SG, Eisenhauer EA, Wanders J, Kaplan RS, Rubinstein L, Verweij J, Van Glabbeke M, van Oosterom AT, Christian MC, Gwyther SG (2000) New guidelines to evaluate the response to treatment in solid tumors. European Organization for Research and Treatment of Cancer, National Cancer Institute of the United States, National Cancer Institute of Canada. J Natl Cancer Inst 92(3):205–216
12. Bernstein D, Lagakos SW (1978) Sample size and power determination for stratified clinical trials. J Stat Comput Simul 8:65–73
13. Bobola MS, Tseng SH, Blank A, Berger MS, Silber JR (1996) Role of O^6-methylguanine-DNA methyltransferase in resistance of human brain tumor cell lines to the clinically relevant methylating agents temozolomide and streptozotocin. Clin Cancer Res 2(4):735–741
14. Esteller M, Garcia-Foncillas J, Andion E, Goodman SN, Hidalgo OF, Vanaclocha V, Baylin SB, Herman JG (2000) Inactivation of the DNA-repair gene MGMT and the clinical response of gliomas to alkylating agents. N Engl J Med 343(19):1350–1354. doi:10.1056/NEJM200011093431901
15. Hegi ME, Diserens AC, Gorlia T, Hamou MF, de Tribolet N, Weller M, Kros JM, Hainfellner JA, Mason W, Mariani L, Bromberg JE, Hau P, Mirimanoff RO, Cairncross JG, Janzer RC, Stupp R (2005) MGMT gene silencing and benefit from temozolomide in glioblastoma. N Engl J Med 352(10):997–1003. doi:10.1056/NEJMoa043331
16. Sonoda Y, Yokosawa M, Saito R, Kanamori M, Yamashita Y, Kumabe T, Watanabe M, Tominaga T (2010) O(6)-Methylguanine DNA methyltransferase determined by promoter hypermethylation and immunohistochemical expression is correlated with progression-free survival in patients with glioblastoma. Int J Clin Oncol 15(4):352–358. doi:10.1007/s10147-010-0065-6
17. van den Bent MJ, Gravendeel LA, Gorlia T, Kros JM, Lapre L, Wesseling P, Teepen JL, Idbaih A, Sanson M, Smitt PA, French PJ (2011) A hypermethylated phenotype is a better predictor of survival than MGMT methylation in anaplastic oligodendroglial brain tumors: a report from EORTC study 26951. Clin Cancer Res 17(22):7148–7155. doi:10.1158/1078-0432.CCR-11-1274
18. Brandes AA, Franceschi E, Tosoni A, Bartolini S, Bacci A, Agati R, Ghimenton C, Turazzi S, Talacchi A, Skrap M, Marucci G, Volpin L, Morandi L, Pizzolitto S, Gardiman M, Andreoli A, Calbucci F, Ermani M (2010) O(6)-methylguanine DNA-methyltransferase methylation status can change between first surgery for newly diagnosed glioblastoma and second surgery for recurrence: clinical implications. Neuro Oncol 12(3):283–288. doi:10.1093/neuonc/nop050
19. Okita Y, Narita Y, Miyakita Y, Ohno M, Fukushima S, Kayama T, Shibui S (2012) Pathological findings and prognostic factors in recurrent glioblastomas. Brain Tumor Pathol. doi:10.1007/s10014-012-0084-2
20. Aldape KD, Wang M, Sulman EP, Hegi M, Colman H, Jones G, Chakravarti A, Mehta MP, Andrews DW, Long L, Diefes K,

Heathcock L, Jenkins R, Schultz CJ, Gilbert MR, Group RTO (2011) RTOG 0525: Molecular correlates from a randomized phase III trial of newly diagnosed glioblastoma. ASCO Annu Meet Proc 29(18_suppl):LBA2000

21. Wick A, Felsberg J, Steinbach JP, Herrlinger U, Platten M, Blaschke B, Meyermann R, Reifenberger G, Weller M, Wick W (2007) Efficacy and tolerability of temozolomide in an alternating weekly regimen in patients with recurrent glioma. J Clin Oncol 25(22):3357–3361. doi:10.1200/JCO.2007.10.7722
22. Quinn JA, Jiang SX, Reardon DA, Desjardins A, Vredenburgh JJ, Rich JN, Gururangan S, Friedman AH, Bigner DD, Sampson JH, McLendon RE, Herndon JE 2nd, Walker A, Friedman HS (2009) Phase II trial of temozolomide plus O^6-benzylguanine in adults with recurrent, temozolomide-resistant malignant glioma. J Clin Oncol 27(8):1262–1267. doi:10.1200/JCO.2008.18.8417
23. Quinn JA, Pluda J, Dolan ME, Delaney S, Kaplan R, Rich JN, Friedman AH, Reardon DA, Sampson JH, Colvin OM, Haglund MM, Pegg AE, Moschel RC, McLendon RE, Provenzale JM, Gururangan S, Tourt-Uhlig S, Herndon JE 2nd, Bigner DD, Friedman HS (2002) Phase II trial of carmustine plus O(6)-benzylguanine for patients with nitrosourea-resistant recurrent or progressive malignant glioma. J Clin Oncol 20(9):2277–2283
24. Stupp R, Mason WP, van den Bent MJ, Weller M, Fisher B, Taphoorn MJ, Belanger K, Brandes AA, Marosi C, Bogdahn U, Curschmann J, Janzer RC, Ludwin SK, Gorlia T, Allgeier A, Lacombe D, Cairncross JG, Eisenhauer E, Mirimanoff RO (2005) Radiotherapy plus concomitant and adjuvant temozolomide for glioblastoma. N Engl J Med 352(10):987–996
25. Brandes AA, Tosoni A, Spagnolli F, Frezza G, Leonardi M, Calbucci F, Franceschi E (2008) Disease progression or pseudoprogression after concomitant radiochemotherapy treatment: pitfalls in neurooncology. Neuro Oncol 10(3):361–367. doi:10.1215/15228517-2008-008
26. van den Bent MJ (2010) Interobserver variation of the histopathological diagnosis in clinical trials on glioma: a clinician's perspective. Acta Neuropathol 120(3):297–304. doi:10.1007/s00401-010-0725-7
27. Hildebrand J, Gorlia T, Kros JM, Afra D, Frenay M, Omuro A, Stupp R, Lacombe D, Allgeier A, van den Bent MJ (2008) Adjuvant dibromodulcitol and BCNU chemotherapy in anaplastic astrocytoma: results of a randomised European Organisation for Research and Treatment of Cancer phase III study (EORTC study 26882). Eur J Cancer 44(9):1210–1216. doi:10.1016/j.ejca.2007.12.005
28. Coons SW, Johnson PC, Scheithauer BW, Yates AJ, Pearl DK (1997) Improving diagnostic accuracy and interobserver concordance in the classification and grading of primary gliomas. Cancer 79(7):1381–1393

Arteriosclerosis, Thrombosis, and Vascular Biology

Journal of the American Heart Association

Application of Infrared Laser to the Zebrafish Vascular System: Gene Induction, Tracing, and Ablation of Single Endothelial Cells

Eiji Kimura, Tomonori Deguchi, Yasuhiro Kamei, Wataru Shoji, Shunsuke Yuba and Jiro Hitomi

Arterioscler Thromb Vasc Biol. 2013;33:1264-1270; originally published online March 28, 2013;
doi: 10.1161/ATVBAHA.112.300602
Arteriosclerosis, Thrombosis, and Vascular Biology is published by the American Heart Association, 7272 Greenville Avenue, Dallas, TX 75231

Print ISSN: 1079-5642. Online ISSN: 1524-4636

Application of Infrared Laser to the Zebrafish Vascular System

Gene Induction, Tracing, and Ablation of Single Endothelial Cells

Eiji Kimura, Tomonori Deguchi, Yasuhiro Kamei, Wataru Shoji, Shunsuke Yuba, Jiro Hitomi

Objective—Infrared laser–evoked gene operator is a new microscopic method optimized to heat cells in living organisms without causing photochemical damage. By combining the promoter system for the heat shock response, infrared laser–evoked gene operator enables laser-mediated gene induction in targeted cells. We applied this method to the vascular system in zebrafish embryos and demonstrated its usability to investigate mechanisms of vascular morphogenesis in vivo.

Approach and Results—We used double-transgenic zebrafish with *fli1:nEGFP* to identify the endothelial cells, and with *hsp:mCherry* to carry out single-cell labeling. Optimizing the irradiation conditions, we finally succeeded in inducing the expression of the mCherry gene in single targeted endothelial cells, at a maximum efficiency rate of 60%. In addition, we indicated that this system could be used for laser ablation under certain conditions. To evaluate infrared laser–evoked gene operator, we applied this system to the endothelial cells of the first intersegmental arteries, and captured images of the connection between the vascular systems of the brain and spinal cord.

Conclusions—Our results suggest that the infrared laser–evoked gene operator system will contribute to the elucidation of the mechanisms underlying vascular morphogenesis by controlling spatiotemporal gene activation in single endothelial cells, by labeling or deleting individual vessels in living embryos. (***Arterioscler Thromb Vasc Biol.* 2013;33:1264-1270.)**

Key Words: endothelial cells ■ gene expression ■ heat-shock response ■ infrared rays ■ morphogenesis ■ zebrafish

The vascular system is necessary for blood supply, thereby providing oxygen and nutrition to all organs. Using time-lapse analysis of living zebrafish embryos transgenic for *fli1:EGFP*, in which the endothelial cells specifically expressed enhanced green fluorescent protein, we studied the formation of the vascular system of the brain during early ontogeny. Our morphological data have indicated that vascular morphogenesis proceeded with a regular time course to form a uniform structure, which led to the subsequent interest in understanding the underlying mechanisms. Although many studies have investigated the morphogenesis of a developing embryo, little is known about the mechanisms underlying the formation of the vascular system. At present, vasculogenesis and angiogenesis have been advocated as being part of vascular development. In vasculogenesis, the primary vascular network was first formed from the lateral plate mesoderm, and then, further blood vessels were generated by both sprouting and nonsprouting angiogenesis. The vascular plexus was rapidly remodeled, and flow dynamics were believed to play critical roles in determining the processes underlying vascular morphogenesis, including the differentiation of arteries and veins.[1] However, the formation of the early vascular network in the developing trunk progressed without blood flow in zebrafish[2]; similar data have been obtained for the vascular development of the brain (unpublished data). These results suggest that vascular morphogenesis is regulated by genetic cues, indicating that precise analysis of gene function is required for its complete understanding.

Several methods have been used to analyze specific gene functions associated with morphogenesis in developing embryos. Recently, the use of conventional knockout mice using the Cre-loxP system[3] or microelectroporated chicken embryos[4] has become common technique. To a certain extent, spatiotemporal gene regulation can be achieved by these methods, whereas strict gene regulation in a single cell is obligatory for the precise understanding of its function, especially in a noncell autonomous system, such as morphogenesis. In contrast, the heat shock protein (*hsp*) promoter has frequently been used for ectopic gene induction in vivo. A combination of the *hsp* promoter and laser irradiation enables the spatiotemporal regulation of gene induction in targeted cells.[5,6] The heat shock response is widely conserved in all organisms,[7] and is thus easily applied to both model and nonmodel organisms in the absence of specific DNA enhancers. The guidance mechanism

Received on: October 5, 2012; final version accepted on: March 10, 2013.

From the Department of Anatomy, Iwate Medical University, Iwate, Japan (E.K., J.H.); Tissue Engineering Research Group, Health Research Institute, National Institute of Advanced Industrial Science and Technology, Hyogo, Japan (T.D., S.Y.); Spectrography and Bioimaging Facility, National Institute for Basic Biology Core Research Facilities, National Institute for Basic Biology, Aichi, Japan (Y.K.); and Department of Project Programs, Institute of Development, Aging and Cancer, Tohoku University, Miyagi, Japan (W.S.).

The online-only Data Supplement is available with this article at http://atvb.ahajournals.org/lookup/suppl/doi:10.1161/ATVBAHA.112.300602/-/DC1.

Correspondence to Eiji Kimura, Department of Anatomy, Iwate Medical University, Iwate 020-3694, Japan. E-mail eijik@iwate-med.ac.jp

Arterioscler Thromb Vasc Biol **is available at http://atvb.ahajournals.org** **DOI: 10.1161/ATVBAHA.112.300602**

of spinal motor axons by *semaphorin 3a1* has been reported using sublethal laser–induced transgene expression in targeted single neurons.[8]

Because this method used a coumarin dye laser (440 nm), it may be suitable to irradiate superficial tissue, but not deep-lying tissue, such as the vasculature. In addition, the mechanism underlying the activation of the *hsp* promoter is still unclear, although the DNA damage induced by laser irradiation might be involved. We thus focused on infrared (IR) laser (1480 nm), which has a superior ability to heat water and can efficiently access deep-lying tissues. The IR laser–evoked gene operator (IR-LEGO) system is a new microscopic method optimized to heat cells by using an IR laser. We confirmed that this system was efficient in regulating spatiotemporal gene expression, and reported IR laser–mediated gene induction in single targeted cells in nematodes (*Caenorhabditis elegans*),[9] and the local gene expression in various tissues, such as the muscle, notochord, and retina in some living vertebrates, for example, zebrafish (*Danio rerio*) and medaka (*Oryzias latipes*).[10]

In this study, we applied this IR-LEGO system to the vascular system in zebrafish and established, to the best of our knowledge, for the first time, an excellent method to induce laser-mediated gene expression in single targeted endothelial cells in vivo. We optimized the irradiation conditions, which resulted in raising the efficiency of laser-mediated gene induction up to 60%. Furthermore, we applied this method to the endothelial cells of the first intersegmental arteries (SeAs) to evaluate the system, and revealed their contribution in connecting the vascular systems of the brain and spinal cord. Our data indicate that the IR-LEGO system is a useful method for the investigation of vascular morphogenesis in vivo.

Materials and Methods

Materials and Methods are available in the online-only Supplement.

Results

IR Laser–Mediated Gene Expression in Targeted Single Endothelial Cells

Previously, we reported IR laser–mediated local gene induction in various tissues in some vertebrates and higher plants.[10] In this study, we attempted to control gene expression in the single endothelial cells in zebrafish. We identified each single endothelial cell by using zebrafish transgenic for *fli1:nEGFP*, and we used the IR laser to irradiate them individually, and induced the expression of mCherry by using the IR-LEGO (Figure 1A–1C). The efficiency of IR laser in targeting the cell was confirmed by observing the reduction of fluorescence intensity (Figure 1D–1F). To optimize the irradiation conditions, we applied various irradiation powers (17.4, 15.6, 13.8, 12.1, and 10.8 mW) to each single SeA endothelial cell for 1 s, respectively. After 18 hours, we evaluated laser-mediated gene induction by using confocal microscopy (Figure 2). Two types of cells expressed mCherry fluorescence after irradiation with various IR laser-power sources: one type included the nontargeted muscle cells that were superficial to the irradiated endothelial cells (Figure 2, arrows), and the other type included the targeted single endothelial cells (Figure 2, arrowheads). To investigate the optimal irradiation conditions, we compared IR laser power–dependent gene induction more precisely; 20 single endothelial cells were irradiated with each laser power condition. The efficiency of gene induction in the targeted and nontargeted cells is summarized in Table 1. The 1-s-long irradiation with IR laser at 17.4, 15.6, 12.8, 12.1, and 10.8 mW could induce gene expression in the targeted single endothelial cells; IR laser irradiation at 12.1 mW achieved the highest efficiency of 30% (6/20). In contrast, gene expression in the nontargeted cells, such as muscle cells, was also confirmed in each irradiated embryo. Suppressing gene induction in the nontargeted cells was difficult under conditions of higher power, such as 17.4 and 15.6 mW (Figure 2A and 2B, and Table 1). However, reducing the irradiation power decreased the efficiency in nontargeted cells (Table 1), and led to the weakening of the fluorescent intensity (Figure 2C–2E). In this case, the 1-s-long irradiation with the 10.8-mW IR laser had the least influence on the nontargeted cells, but the efficiency to induce the expression of mCherry in the targeted cells was inadequate. We, therefore, determined that the 1-s-long irradiation with the 12.1-mW IR laser was the optimal condition to induce gene expression in the endothelial cells, with a lesser influence on the nontargeted cells (Figure 2D and Table 1). Furthermore, we studied the time course of laser-mediated gene expression. We applied various irradiation powers (17.4, 15.6, 13.8, 12.1, and 10.8 mW) to single SeA endothelial cells in the same embryo for 1 s each; mCherry expression was then observed by fluorescence microscopy every 2 hours after irradiation (Figure IIA–IID in the online-only Data Supplement), and 18 hours after

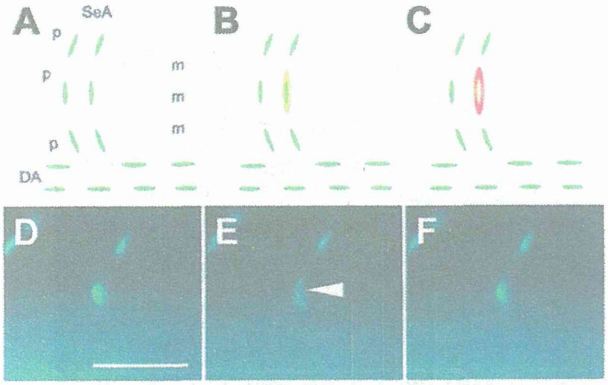

Figure 1. IR laser irradiation procedure for targeting single endothelial cells. **A–C,** Schematic illustration of laser-mediated gene induction in the targeted endothelial cell. IR laser irradiation was carried out under observation with a fluorescent microscope to distinguish the to-be-targeted single endothelial cells labeled with enhanced green fluorescent protein (EGFP) in each nucleus (**A**). They were individually heated, and then, the heat shock protein promoter was activated (**B**). A few hours later, the cytoplasmic expression of mCherry was induced. The irradiated nucleus was finally colored yellow because of superimposition with the nucleus-localized EGFP in a merged fluorescent image (**C**). Pericytes (p) and muscle cells (m) surrounding the vessels could not be observed by fluorescence microscopy. **D–F,** Verification of IR-irradiation could be confirmed by fluorescence. Before (**D**), during (**E**), and after irradiation (**F**). Reduction of the fluorescent intensity of nucleus-localized EGFP was observed only in the heating area during irradiation (**E, arrowhead**). Scale bar, 50 μm. DA indicates dorsal aorta; and SeA, intersegmental artery.

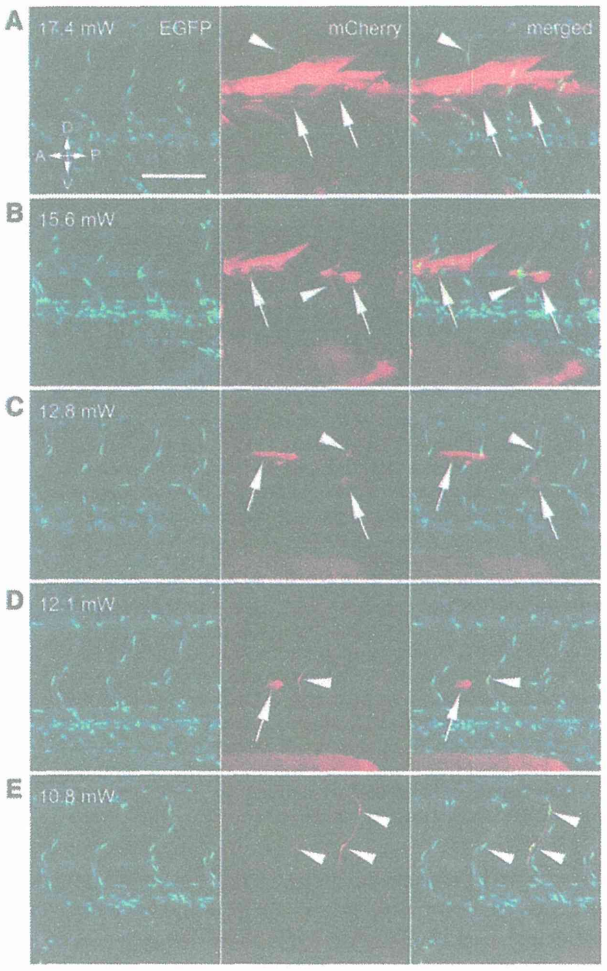

Figure 2. IR laser power–dependent mCherry expression in targeted and nontargeted cells. We applied irradiation with an IR laser at 17.4 mW (**A**), 15.6 mW (**B**), 12.8 mW (**C**), 12.1 mW (**D**), and 10.8 mW (**E**) for 1 s to the targeted single endothelial cells, and observed them with confocal microscope 18 hours later. Gene induction of mCherry in the targeted endothelial cells (arrowheads) and nontargeted cells (**arrows**). The direction of the embryo is indicated. Scale bar, 100 μm. A indicates anterior; D, dorsal; P, posterior; and V, ventral.

irradiation by confocal microscopy (Figure IIE–IIG in the online-only Data Supplement). The first 2 irradiations at 17.4 and 15.6 mW resulted in mCherry induction only in the nontargeted muscle cells (Figure IIF and IIG in the online-only Data Supplement, arrows), whereas the fourth irradiation at 12.1 mW succeeded in inducing laser-mediated gene expression in the targeted single endothelial cell (Figure IIF and IIG in the online-only Data Supplement, arrowheads). The expression of mCherry in the nontargeted muscle cells was mild at 4 hours after the irradiation (Figure IIB in the online-only Data Supplement, arrows), but grew stronger with time (Figure IIC and IID in the online-only Data Supplement, arrows). The targeted endothelial cell also expressed mCherry 6 hours after irradiation, which also grew stronger (Figure IIC and IID in the online-only Data Supplement, arrowheads). These observations will be valuable to assess the effect of the expression of particular genes in endothelial cells by using this system.

Table 1. Efficiency of Laser-Mediated Gene Induction at Various Infrared Laser Powers

Condition of Irradiation (1-s-Long Single Pulse), mW	Gene Induction in Targeted Endothelial Cells	Gene Induction in Nontargeted Cells
17.4	2/20 (10%)	20/20 (100%)
15.6	3/20 (15%)	18/20 (90%)
12.8	2/20 (10%)	10/20 (50%)
12.1	6/20 (30%)	4/20 (20%)
10.8	3/20 (15%)	2/20 (10%)

The number of mCherry-induced endothelial cells and mCherry-induced nontargeted cells, and the percentage of each count are indicated.

Efficiency of IR Laser–Mediated Gene Induction

As we succeeded in optimizing the irradiation conditions to induce laser-mediated gene expression in single targeted endothelial cells with minimum effect on nontargeted cells, we next investigated its efficiency by using this optimized condition (12 mW for 1 s). We selected 1 endothelial cell from each SeA, and in total, 70 single endothelial cells from the SeAs at 2 dpf were irradiated. As a result, the gene expression of mCherry was induced in 25 irradiated single endothelial cells with an efficiency of 35.7% (25/70). The expression in nontargeted cells was also observed, and its efficiency was 12.9% (9/70). We then decreased the irradiation power from 12 mW to 10.8 mW and increased the frequency from 1 time to 3 times (pulsed irradiation) to further improve efficiency. Under these conditions, we used the IR laser to completely irradiate 30 single endothelial cells. As a result, the gene expression of mCherry was induced in 18 irradiated endothelial cells, that is, the efficiency increased to 60% (18/30). Accordingly, the gene expression in nontargeted cells also increased to 33.3% (10/30). These results are summarized in Table 2, and select images of irradiated embryos in 2 different conditions have been presented as examples (Figures III and IV in the online-only Data Supplement). Comparison of these results suggests an inconvenient relationship, whereby increasing the frequency of irradiation significantly improves the efficiency of laser-mediated gene induction in the targeted cells, whereas the induction in nontargeted cells increased at the same time. However, the maximum induction rate of 60% was an adequate achievement with respect to controlling spatiotemporal gene expression in vivo. Our data suggest that the IR-LEGO system will be a powerful tool for the functional analysis of a particular gene in vivo associated with vascular morphogenesis, especially for a system that satisfies the requirement of complete deletion of gene induction in nontargeted cells.

Tracing the Targeted Single Endothelial Cells of the First Intersegmental Arteries

The induction of mCherry in the targeted endothelial cells enabled us to trace them throughout the ontogeny within the period of mCherry expression. We used this advantage to analyze the formation of the connecting portion of the vascular systems between the brain and spinal cord. Morphogenesis in this region has previously been reported using microangiography, and it showed that the primordial hindbrain channel (PHBC) and basilar artery (BA) extended caudally and connected with

Table 2. Efficiency of Laser-Mediated Gene Induction Under Optimized Conditions

Condition of Irradiation	Gene Induction in Targeted Endothelial Cells	Gene Induction in Nontargeted Cells
1-s-long single pulse of 12 mW laser	25/70 (35.7%)	9/70 (12.9%)
1-s-long 3 pulses of 10.8 mW laser (total, 3 s)	18/30 (60%)	10/30 (33.3%)

The number of mCherry-induced endothelial cells and mCherry-induced nontargeted cells, and the percentage of each count are indicated.

the dorsal longitudinal anastomotic vessel (DLAV) at 1.5 to 2.0 dpf, which was formed by the longitudinal anastomosis of the branches of the intersegmental vessels in the dorsal region of the neural tube (schematic illustrations are indicated in Figure 3A and 3B).[11] However, this method allowed the observation of only the lumen of the vessels, not the growing vessels before tube formation, and therefore, it is still unknown how these vessels were connected. We focused on the first SeAs as the candidate connecting these vascular systems, because their contribution to this connection had not been revealed. They could be observed obviously in the *fli1:nEGFP* transgenic zebrafish embryos (Figure 3C), although they could not be identified by microangiography (Figure 3A). To investigate their role in this connection, we labeled and traced them after irradiation with the IR laser. After 16 to 18 hours, we confirmed the localization of the green/red fluorescence-labeled endothelial cells dorsally and laterally after these vessels became connected (Figure 3D and 3E). We applied 2 irradiating conditions for these labeling experiments; a 1-s-long single pulse from a 12-mW laser and three 1-s-long pulses with a 10.8-mW laser (pulse irradiation). The efficiency labeling of the first SeA of the former condition was 16.7% (3/18), and that of the latter was 20% (2/10). In total, we succeeded in labeling 5 targeted endothelial cells of the first SeAs, and the mCherry-labeled cells from the first SeAs were located in the connecting portion of the BA, PHBC, and DLAV, suggesting that the endothelial cells of first SeAs bridge the vascular systems of the brain and spinal cord. Our labeling data for the first SeAs are summarized in Figure 3F and 3G, and we assume that the first SeAs could not be represented by microangiography because of the lack of connection with the dorsal aorta.

Ablation of the Endothelial Cells in the First Segmental Arteries

Because IR-laser is capable of heating water, irradiation overdose can cause injury to the cells. We used this property to ablate particular vessels in the formation of the vascular system. For the first target of the ablation study, we again selected the first SeA. We applied a high-power flash irradiation of IR laser (70 mW for 8-ms) to the endothelial cells, and evaluated its influence over the morphogenesis of the vascular systems between the brain and spinal cord. Whether this attempt to ablate the targets succeeded was judged by the disappearance of nucleus-localized enhanced green fluorescent protein. The change in the connecting portion of the BA, PHBC, and DLAV was observed by confocal microscopy 16 to 18 hours after ablation, in both lateral and dorsal views (Figure 4A and 4B). Although PHBC usually extends obliquely from the caudal head region to the dorsal end of the second SeA, PHBC on the irradiated side did not connect to the second SeA; that is, their extension stopped around the ablated first SeA (Figure 4, black arrows). Furthermore, the connection of the BA and DLAV on the irradiated side diminished (Figure 4, white arrowheads), and alternatively, the collateral blood vessel formed between the BA and PHBC (Figure 4, black arrowheads), whereas the BA in the nonirradiated side connected to the DLAV bending laterally (Figure 4, white arrows). We totally ablated 7 embryos (with the following condition: 70 mW, 8 ms) and observed the effects. The PHBC and DLAV of the ablated side were not connected in all the embryos (Figure 4, black arrows), whereas the bridge between the BA and DLAV (Figure 4, white arrowheads) diminished in 6 of the embryos. (In the rest, the ectopic vessel from the collateral vessel between the BA to PHBC connected to the DLAV.) To reconfirm the vascular formation of the ablated and nonablated first SeAs, we performed confocal microangiography. As a result, the disconnection between the BA, PHBC, and DLAV was clearly demonstrated on the ablated side (Figure V in the online-only Data Supplement). These ablation data for the first SeA are summarized in Figure 4C and 4D. To examine the influence of the overdose of irradiation to the surrounding tissues, we observed the targeted single endothelial cells by both bright-field and fluorescent microscopy before and after the irradiation (Figure VI in the online-only Data Supplement). After the ablation, the nuclear-localized fluorescence in the targeted cell weakened and finally diminished. Burn injury of the ablated cell was also confirmed in the bright-field image, whereas obvious defects to the cells in the surrounding tissues, such as the somites and neural tubes, could not be observed (we confirmed diminishment of the connecting vessels in this embryo). Furthermore, we stained some ablated embryos by 4',6-diamidino-2-phenylindole 16 to 18 hours after the ablation and observed it using confocal microscopy (Figure VII in the online-only Data Supplement). The obvious difference between the ablated and nonablated sides could not be confirmed. Taken together, the vessels diminished by the ablation of the first SeAs were well corresponded to the labeled vessel in Figure 3; therefore, these data are also useful to investigate the contribution of the first SeAs in the vascular morphogenesis between the brain and spinal cord.

Discussion

We applied the IR-LEGO system to the zebrafish vascular system to establish spatiotemporal gene regulation. Previous studies using electroporation,[4] point laser,[6] and the IR-LEGO system[10] enabled only local gene regulation in vertebrates. In this study, we isolated each endothelial cell by using nucleus-localized enhanced green fluorescent protein and optimized the irradiation conditions needed to decrease gene induction in nontargeted cells. Thus, we achieved precise control of gene expression in single endothelial cells, which were extreme thin and contiguously surrounded by pericytes and muscle cells (Figure 2). Another single-cell gene expression system in zebrafish using a high-power pulse laser has recently been

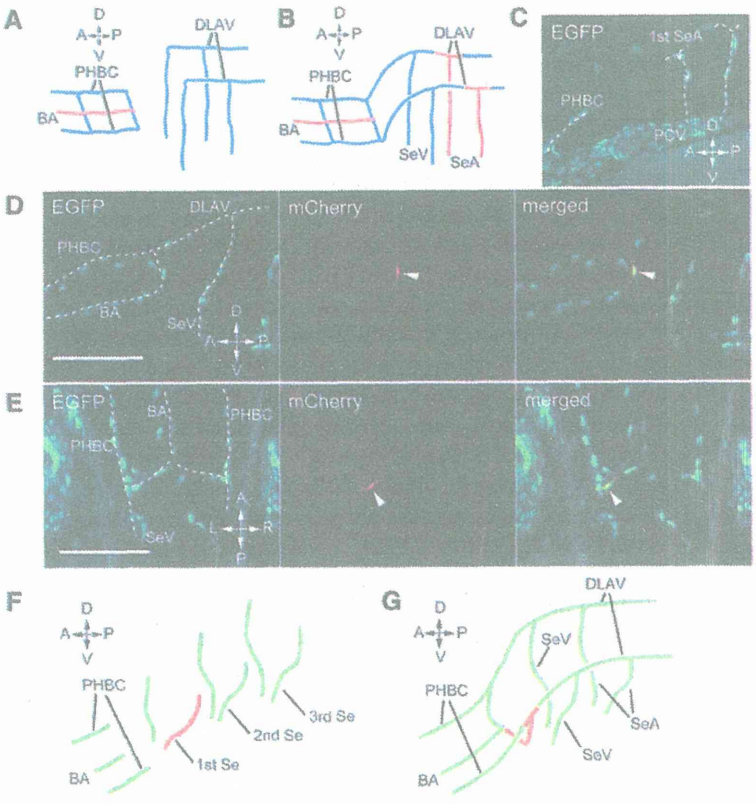

Figure 3. Integration of the vascular systems in the brain and spinal cord. **A** and **B**, Schematic illustrations of brain–spinal cord bridging at 1.5 dpf (**A**) and 2.0 dpf (**B**). This connection was formed in this period.[11] **C**, Endothelial cells of the first intersegmental artery (SeA; asterisks) and primordial hindbrain channel (PHBC) extending caudally in the *fli1:nEGFP* transgenic zebrafish embryo at 1.5 dpf before bridging. **D** and **E**, We labeled embryos at 1.5 dpf by using the infrared laser–evoked gene operator system through irradiation with three 1-s-long pulses from a 10.8-mW laser. The single endothelial cell of the first SeA labeled by laser-mediated gene induction of mCherry located in the bridging portion of basilar artery (BA) and dorsal longitudinal anastomotic vessel (DLAV; 18 hours after irradiation). Lateral view (**D**) and dorsal view (**E**). **F** and **G**, Schematic illustrations of labeling examination of first SeA at 1.5 dpf (**F**) and 2.0 dpf (**G**). The endothelial cells of the targeted first SeA are in red. **C–G**, Direction of the embryo is indicated for each figure. Scale bar, 100 μm. A indicates anterior; D, dorsal; L, left; P, posterior; PCV, posterior cardinal vein; R, right; Se, intersegmental vessel; SeV, intersegmental vein; and V, ventral.

reported.[12] This system uses physical impulses of pulse irradiation for transferring injected material to the target cells from the surroundings, hence requires DNA or mRNA microinjection to the neighboring area for gene expression. This system does not require transgenic strains; hence, it is suitable for a nonmodel animal, but is not appropriate for our objectives. Recently, we revealed how the vasculature in the brain was developed during early ontogeny by time-lapse analysis (unpublished data). Gene regulation in the targeted single endothelial cells in vivo will enable the analysis of the influence of a particular gene over the morphogenesis of each vessel in these regions.

Repeating the irradiation several times improved the efficiency of gene induction and led to a maximum induction rate of 60% (Table 2). However, the induction rate of nontargeted cells also rose by 3-fold. When the IR laser was used for irradiation, the endothelial cells shrunk as if evading the heat stress. The surrounding muscle cells may also contract after

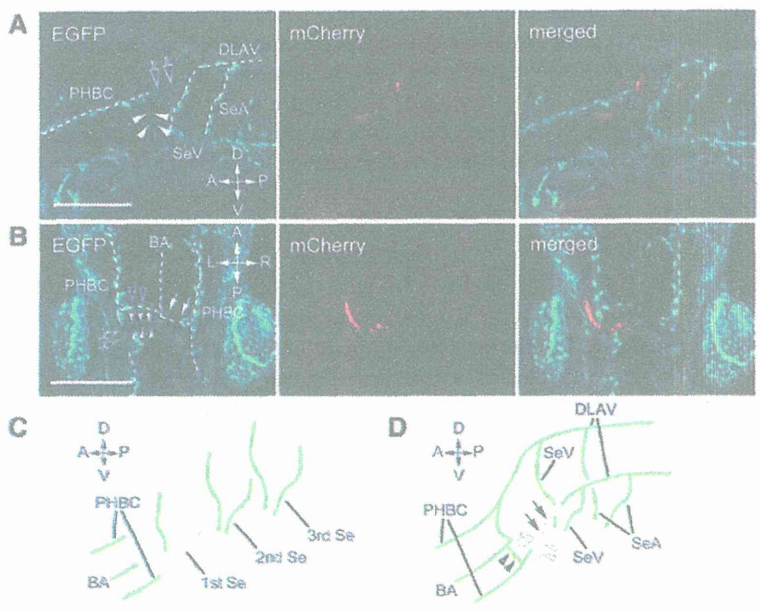

Figure 4. The connection of the vascular systems of the brain and spinal cord changed after the ablation of the first intersegmental artery (SeA). **A** and **B**, We ablated all endothelial cells of the unilateral first SeA using the infrared laser–evoked gene operator system, and observed them with CLSM 18 hours after the ablation. The gene expression of mCherry in the surrounding tissue was observed only on the ablated side. Lateral (**A**) and dorsal (**B**) views. On the ablated side, the bridging portions of the basilar artery (BA) and dorsal longitudinal anastomotic vessel (DLAV; **A** and **B** white arrowheads), and the primordial hindbrain channel (PHBC) and DLAV (**A** and **B** black **arrows**) diminished, and instead, the collateral vessel from the BA to PHBC formed (**B**, black arrowheads). **C** and **D**, Schematic illustrations of the ablation examination of the first SeA at 1.5 dpf (**C**) and 2.0 dpf (**D**). Normal vasculature that diminished on the ablated side is shown by a dotted gray line. **A–D**, The direction of the embryo is indicated in each figure. Scale bar, 100 μm. A indicates anterior; D, dorsal; L, left; P, posterior; PCV, posterior cardinal vein; R, right; Se, intersegmental vessel; SeV, intersegmental vein; and V, ventral.